atmosphere

MDPI

Article

Numerical Investigation of Ultrafine Aerosol Deposition inside a Needle Charger without Applied Voltage

Cheng-Hsiung Huang [1,*] and Yu-Hsiang Cheng [2,3,4]

[1] Department of Environmental Engineering and Health, Yuanpei University of Medical Technology, Hsinchu 300102, Taiwan
[2] Department of Safety, Health and Environmental Engineering, Ming Chi University of Technology, Taishan, New Taipei 243089, Taiwan; yhcheng@mail.mcut.edu.tw
[3] Center for Environmental Sustainability and Human Health, Ming Chi University of Technology, Taishan, New Taipei 243089, Taiwan
[4] Chronic Diseases and Health Promotion Research Center, Chang Gung University of Science and Technology, Puzi, Chiayi 613016, Taiwan
* Correspondence: chhuang@mail.ypu.edu.tw

Abstract: The deposition of ultrafine aerosols with a size range of 3–20 nm in a needle charger has been studied numerically by simulating the flow field and the particle trajectory. The calculation model explored the particle deposition in the needle charger without applied voltage for various particle diameters, flow rates, entrance radial positions and deposition axial distances. It is first quantitatively proposed that most of the particles are attached to the outer electrode wall instead of the needle electrode wall for different flow rates and particle diameters. It is found that the numerical results of the particle deposition of the needle charger are consistent with previous experimental data. Moreover, the results demonstrate that reducing the flow rate increases the particle deposition of the needle charger. The numerical models explain and quantify the particle deposition and its attachment position for the needle charger without applied voltage.

Keywords: ultrafine aerosols; deposition; needle charger

Citation: Huang, C.-H.; Cheng, Y.-H. Numerical Investigation of Ultrafine Aerosol Deposition inside a Needle Charger without Applied Voltage. *Atmosphere* **2022**, *13*, 695. https://doi.org/10.3390/atmos13050695

Academic Editors: Fernanda Isabel Oduber Pérez and Estela D. Vicente

Received: 28 March 2022
Accepted: 26 April 2022
Published: 27 April 2022

1. Introduction

Ultrafine aerosols in the air may cause potentially adverse effects on the environment and human health and have caused extensive research and discussion in recent years [1–4]. In the studies of air pollution and public health, the measurement of the particle size distribution and number concentration of nanoparticles is very important. Differential mobility analysis is a common instrument used to measure the particle size distribution and number concentration of these ultrafine aerosols [5,6]. Since the particle size measuring instrument through electro-differential mobility analysis requires the particles to have a unipolar charge with a known charge distribution, it is necessary to explore the charged and uncharged behavior of ultrafine aerosols for some corona chargers [7–9].

The corona chargers use a non-uniform electrostatic field between the needle and the wall or between the wire and the tube and have been applied to charged particles as the first step in electrical mobility analysis [10–12]. The direct needle charger in these corona dischargers has the advantages of simple design, easy manufacturing and low cost. To know the charged distribution of particles for the application of the needle charger, it needs to pay attention to its high charging efficiency and low particle loss [13–15]. Alonso et al. [16] conducted an experimental method containing many parameters to measure the performance of the needle charger, including intrinsic and extrinsic charging efficiencies, as well as diffusion and electrostatic particle losses. The research results showed that the extrinsic and intrinsic charging efficiencies were important parameters in the applications of the needle charger. In addition, the electrostatic loss of the needle charger increased with an

increasing charger voltage, while the diffusion loss decreased. When the needle charger was turned off, the diffusion loss in the charger reached the maximum value. Although experimental studies have utilized increased flow rates to reduce the particle deposition, a quantitative analysis of the ultrafine aerosol deposition inside the needle charger without applied voltage has not been fully reported in the literature. In addition, the influences of particle sizes and flow rates on the distances of ultrafine aerosols adhering to the electrode wall are also lacking.

For improving the charging efficiency of the needle charger, the particle depositions caused by diffusion and electrostatic effects have become an important issue. Many studies have shown that the charging efficiency of the needle charger can be improved by reducing the loss of ultrafine particles inside the needle charger [15–18]. Some researchers employed an additional sheath air to shroud the aerosol to reduce the particle diffusion deposition of the charger [19]. However, the use of this method must consider that the design was more complicated, and the aerosol concentration was diluted at the charger outlet. Therefore, the calculations of the ultrafine aerosol depositions and trajectories within the simple charger without applied voltage are well worth exploring. Furthermore, it is important to see if the ultrafine aerosol trajectories closely follow the flow field when the corrected Stokes drag force and the Brownian force are considered, because it can have a significant effect on the particle deposition in the needle charger.

Recently, Alonso and Huang [20] evaluated a needle charger for efficient charging of particles with a diameter of a few nanometers. Research results showed that the needle charger with a smaller effective volume caused smaller nanoparticle diffusion depositions. Since the electrostatic and diffusion losses of ultrafine aerosols inside the needle charger were reduced, the extrinsic charging efficiency of the needle charger was improved. Intra et al. [21] evaluated the charging efficiencies and losses of ultrafine particles with the size range of 15–75 nm for a unipolar corona-based ionizer. Their results showed that smaller particles will have higher diffusion deposition than larger particles due to Brownian diffusion effect. In addition, for particles with a particle diameter greater than 20 nm, the Brownian diffusion losses were negligible. However, it was difficult to quantify the relative contribution of the particle's attachment positions to the diffusional deposition in the needle charger under different flow rates, especially for the ultrafine aerosols smaller than 10 nm. Therefore, the purpose of this study is to construct a method to investigate the influences of particle diffusional trajectories on attachment positions and ultrafine aerosol depositions in the needle charger. A numerical model was employed to calculate the diffusion deposition of uncharged particles in the needle charger. The ultrafine aerosol deposition in the needle charger without applied voltage was investigated numerically by simulating the flow field and particle trajectory for different particle diameters, flow rates, entrance radial positions and deposition axial distances.

2. Methods

Figure 1 depicts the schematic diagram of the needle charger in this investigation. The charger was composed of an outer electrode with a conical shape and an inner electrode with a sharp point end. The inner electrode was designed to use the stainless steel, so high voltages could be applied to the electrode. The conical outer wall coaxial with the electrode was designed with the grounded metal material. The radii of the inlet, r_1, and outlet, r_3, for the conical sections are 1 cm and 0.175 cm, respectively. The radius of the needle electrode, r_2, is 0.15 cm, and the height of the cone is 2 cm. The design dimensions were based on the studies of nanoparticle loss measurements in corona chargers [16]. It was originally expected to help reduce nanoparticle diffusion losses by moving the electrode holder at the particle inlet. The results showed that the nanoparticle loss through the sidewall was approximately the same as the presence of the electrode holder. However, the manufacture of a non-fixed electrode holder was easier to carry out. This study adopted a geometric design similar to that of the non-fixed electrode holder. The numerical results could therefore be compared with the experimental data. Calculations of the fluid flow fields and

particle trajectories inside the needle charger without power supply were performed under different conditions. For the calculation of flow field inside the uncharged needle charger, it was simulated by solving two-dimensional continuity and Navier–Stokes equations assuming steady, incompressible, axisymmetric, viscous and laminar fluid flow. Figure 2 is the main numerical domain used to calculate the flow field of the needle charger. The outer electrode wall and needle electrode wall are set as solid boundary conditions. Three grid numbers of 21,000, 84,000 and 336,000 were used in the computational domain to test the grid independence. When the number of grids was increased from 21,000 to 84,000, the particle deposition in the needle charger without applied voltage for 3 nm particles at 2 L min^{-1} changed from 25.2% to 27.4%. When the number of grids was increased from 84,000 to 336,000, the particle deposition changed from 27.4% to 27.7%. The number of grids varied from 84,000 to 336,000 resulting in a difference of only 0.3% in the calculated results. Therefore, a total of 84,000 (200 in the r-direction × 420 in the z-direction) non-uniform rectangular grids were used during the computational simulation. Air is assumed to be at 20 °C and 1 atm. The governing equations are discretized using the finite volume method and solved by the SIMPLE algorithm [22].

$$\frac{1}{r}\frac{\partial}{\partial r}(ru_r) + \frac{\partial u_z}{\partial z} = 0 \tag{1}$$

$$\rho_a\left(u_r\frac{\partial u_r}{\partial r} + u_z\frac{\partial u_r}{\partial z}\right) = -\frac{\partial P}{\partial r} + \mu_a\left[\frac{1}{r}\frac{\partial}{\partial r}\left(r\frac{\partial u_r}{\partial r}\right) + \frac{\partial^2 u_r}{\partial z^2}\right] - \frac{\mu_a u_r}{r^2} \tag{2}$$

$$\rho_a\left(u_r\frac{\partial u_z}{\partial r} + u_z\frac{\partial u_z}{\partial z}\right) = -\frac{\partial P}{\partial z} + \mu_a\left[\frac{1}{r}\frac{\partial}{\partial r}\left(r\frac{\partial u_z}{\partial r}\right) + \frac{\partial^2 u_z}{\partial z^2}\right] \tag{3}$$

where u_r and u_z is the air velocity in r (radial) and z (axial) direction, respectively, ρ_a is the air density, P is the pressure, and μ_a is the air viscosity.

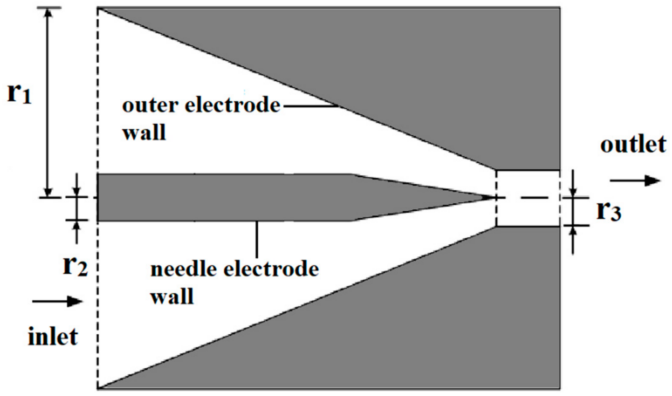

Figure 1. Sketch of the needle charger.

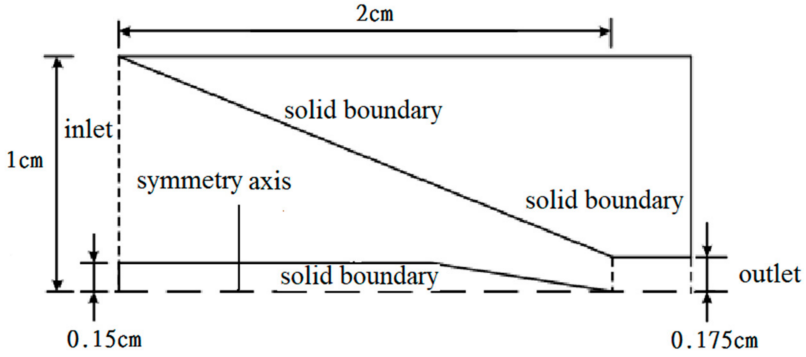

Figure 2. Numerical domain of calculation in the needle charger.

After calculating the flow field, the particle motion equation is integrated using the fourth-order Runge–Kutta method. The particle motion equation is governed by the following:

$$\frac{d\vec{v_p}}{dt} = \vec{f_d} + \vec{f_b} \tag{4}$$

where $\vec{f_d}$ is the drag force per unit mass, $\vec{f_b}$ is the Brownian force per unit mass, and $\vec{v_p}$ is the particle velocity.

The drag force per unit mass including Cunningham correction in the particle motion equation is described by Stokes's law as [23]:

$$\vec{f_d} = \frac{3\mu_a}{4D_p^2\rho_p C} C_d Re_p \left(\vec{v_a} - \vec{v_p}\right) \tag{5}$$

where C_d is the empirical drag coefficient, Re_p is the particle Reynolds number, D_p is the particle diameter, C is the Cunningham correction factor, ρ_p is the particle density and $\vec{v_a}$ is the air velocity.

For the ultrafine aerosols suspended in a fluid and subjected to the random impact of unbalanced gas molecules, the Brownian motion in an irregular path is described by a zero mean Gaussian random process [24,25]:

$$\vec{f_b} = G\sqrt{\frac{\pi S}{\Delta\tau}} \tag{6}$$

$$S = \frac{2D\beta^2}{\pi} \tag{7}$$

where $\beta = 3\pi\mu_a D_p / Cm_p$ is the inverse of the particle relaxation time, $D = KTC/3\pi\mu_a D_p$ is the diffusion coefficient, m_p is the particle mass, $\Delta\tau$ is the time step, G is the zero mean unit variance Gaussian random number given by $G_1 = \sqrt{-2lnx_1}cos(2\pi x_2)$ and $G_2 = \sqrt{-2lnx_1}sin(2\pi x_2)$, and x_1 and x_2 are the pairs of uniform random numbers. The time step in the calculation should be chosen as much smaller than the relaxation time of the particles. Such a small enough time step keeps the drag force approximately constant during the interval, so the integral error of the particle motion equation is very small.

If the velocity profiles and particle concentration at the inlet of the needle charger are assumed to be uniform and we suppose the particles are collected when they reach the wall, then the ultrafine aerosols deposition in the charger equals the outer electrode deposition, d_{outer}, plus the needle electrode deposition, d_{needle}, which can be calculated as:

$$d_{outer} = \frac{r_1^2 - r_{c1}^2}{r_1^2 - r_2^2} \tag{8}$$

$$d_{needle} = \frac{r_{c2}^2 - r_2^2}{r_1^2 - r_2^2} \tag{9}$$

where r_{c1} and r_{c2} represent the critical collection radius of the particles for the outer electrode and the needle electrode, respectively. The particles entering the needle charger in the radial direction between r_{c1} and r_1, or r_{c2} and r_2 will adhere to the outer electrode or the needle electrode wall.

In the calculation of the fluid flow fields and particle trajectories in the needle charger without power supply, the interaction between particles is ignored. When particles are introduced into the system to obtain their trajectories, it is assumed that the particles are spherical and the presence of particles does not affect the fluid flow field. The particle mass of 3–20 nm ultrafine aerosols is assumed to be $3.06 \times 10^{-14} - 9.07 \times 10^{-12}$ μg. In addition, the flow field inside the needle charger without a power supply is assumed to be axisymmetric and there is no flow in the azimuth direction. Therefore, when the

particle passes through the aerodynamic system of the needle charger, the calculation of the trajectory in the (r, z) plane is sufficient to give a statistically reasonable result of the particle deposition inside the needle charger.

3. Results and Discussion

3.1. Particle Motion inside Charger

To obtain the diffusion adhesion and the deposition of ultrafine aerosols, this study calculated the flow field and particle trajectories inside the needle charger without applied voltage. Figure 3 shows the streamlines in the charger without power supply at a flow rate of 2 L min^{-1}. The airflow enters the charger from the inlet and gradually accelerates until it leaves the charger and reaches the maximum value. From the development of the flow velocity profile inside the charger, there is a lower velocity distribution near the walls of the outer electrode and needle electrode, while a higher velocity value is found close to the center of the airflow. Figure 4 shows the trajectory of particles with diameters of 3 nm, 5 nm and 10 nm releasing at different radial positions (r_p) at a flow rate of 2 L min^{-1}. For the particles introduced close to the outer electrode (r_p/r_1 = 0.9), the trajectory of the 3 nm nanoparticle significantly drifts away from the streamline driven by the particle diffusion force, and it is deposited on the outer electrode wall.

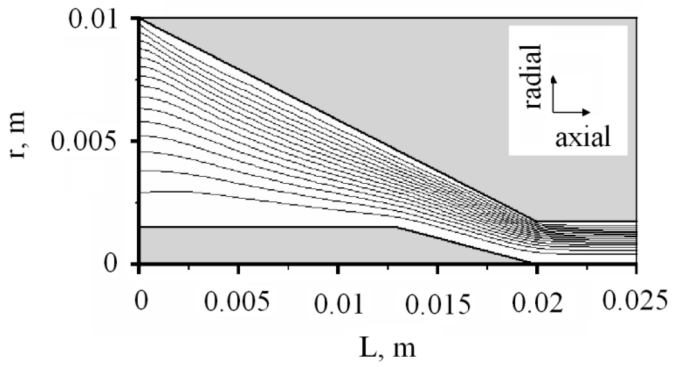

Figure 3. Streamlines inside the needle charger for the flow rate of 2 L min^{-1}.

On the contrary, the particles with a diameter of 10 nm can leave the charger without being lost to the wall due to the diffusion force not being enough to bring them close to the wall. The trajectories of the particles with a diameter of 5 nm also deviate from the streamline by a diffusion force and deposits on the wall of the external electrode. Compared with the trajectories of the 3 nm particles, it is found that 5 nm particles move for longer and their attachment positions are closer to the downstream area. In the case of particles introduced close to the centerline (r_p/r_1 = 0.5), three particle sizes leave the charger without adherence to the wall. It is seen that 3 nm particle trajectories drift more significantly in the early stage than the other two particles. When they reach the downstream region, the Brownian motion mechanism of the particles reduces due to the acceleration of the airflow, and the particle trajectories gradually tend to the corresponding streamline.

For particles entering close to the needle electrode (r_p/r_1 = 0.2), the trajectories of 3 nm nanoparticles deviate from the streamline by the diffusion force, and then adhere to the wall of the needle electrode. However, the particles with a diameter of 5 nm and 10 nm survive the diffusion deposition process and pass through the charger smoothly without depositing on the needle electrode wall. In general, the trajectory of the smaller particles (3 nm) moves closer to the wall, while the trajectory of the larger particles (10 nm) approaches closer to the corresponding streamline. Notably, this study solves the movement of ultrafine aerosols under the combined forces of corrected Stokes drag and Brownian force. Hence, it is informative to provide a comparison of the two forces for ultrafine aerosols with various particle sizes, so as to understand the underlying physics more easily. Furthermore, this study is also useful for exploring how ultrafine aerosols follow the flow field. For ultrafine

aerosols, it is worth investigating in the future to see if the particles will closely follow the flow field inside the charger when only the corrected Stokes drag is considered.

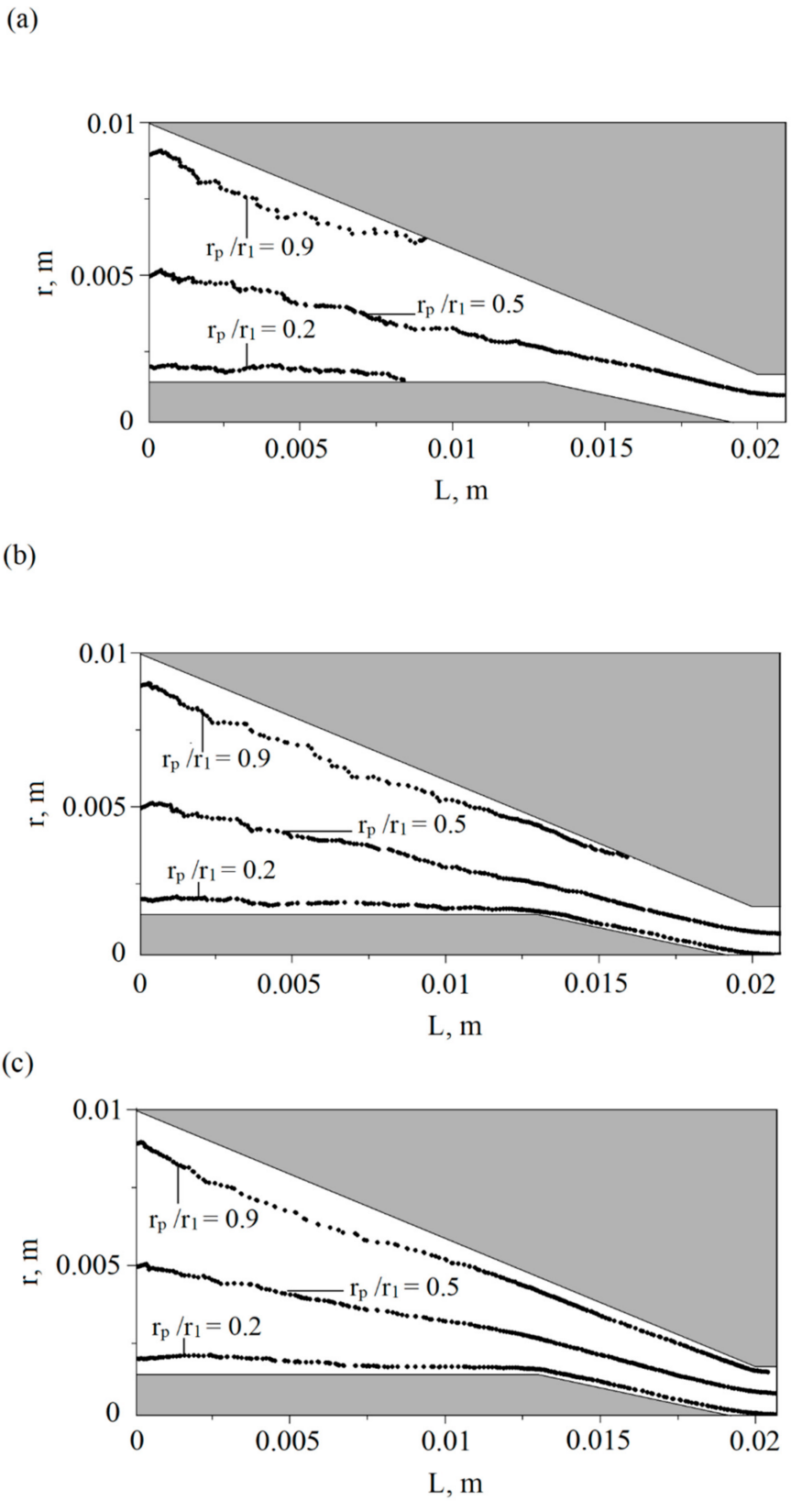

Figure 4. Particle trajectory inside the needle charger for the particle diameters of (**a**) 3 nm, (**b**) 5 nm and (**c**) 10 nm at the flow rate of 2 L min^{-1}.

3.2. Ultrafine Aerosols Deposition

The numerically obtained results of the particle deposition in the needle charger are compared with the experimental data in the literature [16], shown in Figure 5. The plot demonstrates that the deposition of particles predicted by the present numerical model is close to the experimental data for the flow rate of 2.0 L min^{-1}. The figure also shows that the deposition fraction of particles in the needle charger without applied voltage is close to the fraction of particles lost by diffusion to the wall of the needle charger with various voltages. After corona discharge occurs, the proportion of intrinsically charged particles increases as the voltage increases, while the diffusion loss of particles decreases with the increase in voltage. Intrinsic charging efficiency is defined as the ratio of charged particles to originally neutral particles inside the charger [16]. Although the diffusion losses decrease with increasing voltage, the proportion of remaining uncharged particles also decreases. In this situation, the diffusion losses will be close to each other regardless of whether the chargers are turned on or off. Additionally, for a charger without an applied electric field or when the charger works at a voltage lower than the voltage required for corona onset, the diffusional penetrations of uncharged particles are similar to one another.

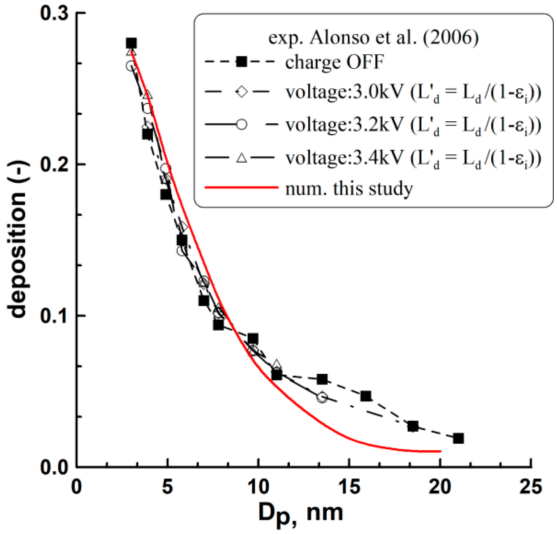

Figure 5. Comparison of numerical deposition in the needle charger with experimental data [16] (L'_d: diffusion loss, charger OFF, L_d: diffusion loss, charger ON, ε_i: intrinsic efficiency).

3.3. Effect of Flow Rate

This study then examines the effect of flow rate on the particle deposition of the needle charger. Figure 6 shows the particle deposition in the needle charger as a function of the particle diameter for the flow rates of 1 L min^{-1}, 2 L min^{-1} and 4 L min^{-1}. For the needle charger at operating flow rates of 1, 2 and 4 L min^{-1}, the inlet flow velocity is 5.4, 10.8 and 21.7 cm s^{-1}, and the Reynolds number, $Re = \rho_a U_0 (R_1 - R_2)/\mu_a$ (U_0: inlet average flow velocity, R_1: the diameter of the inlet, R_2: the diameter of the needle electrode) is 61, 122 and 245, respectively. It is seen that the particle deposition decreases with increasing values of the particle diameter inside the needle charger for various flow rates. For the particles with a diameter of 3 nm, the particle deposition within the needle charger is about 33.4% at a flow rate of 1 L min^{-1}, and it is reduced to about 15.7% at a flow rate of 4 L min^{-1}. This is because the increasing flow rate of the needle charger reduces the diffusion time available for particles to reach the wall. For example, the diffusion time is 0.156, 0.078 and 0.039 s for the needle charger with a flow rate of 1, 2 and 4 L min^{-1}, respectively. For 15 nm particles, the particle deposition is about 2.9% at the flow rate of 1 L min^{-1}, and about 0.5% at the flow rate of 4 L min^{-1}. Since the diffusion for larger particles becomes weaker, the effect of flow rate on the particle deposition is less significant.

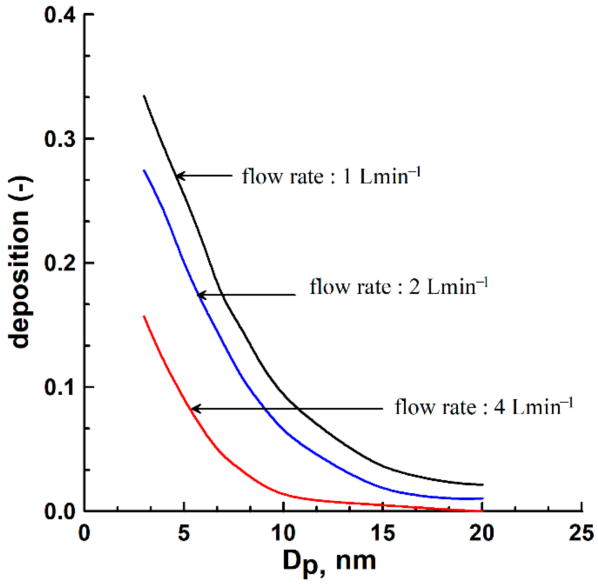

Figure 6. Deposition in the needle charger for various particle diameters and flow rates.

In general, the particle deposition in the needle charger with a larger flow rate is lower than that with a smaller flow rate. It is worth noting that the increase in flow rate reduces the diffusion time of particles within the needle charger and reduces the effective collisions between particles and ions, which affects its intrinsic charging efficiency. The intrinsic charging efficiency represents the proportion of neutral particles charged in the charger, regardless of whether they subsequently survive the deposition of particles in the needle charger.

3.4. Position of Particle Deposition

Figure 7 shows the percentage of particle deposition on the outer electrode wall and needle electrode wall of the needle charger at different flow rates. This figure shows that most of the particle deposition occurs in the outer electrode area for different particle sizes and flow rates. The particle deposition for the particle diameter of 3 nm on the outer electrode wall at the flow rate of 1 L min^{-1} and 2 L min^{-1} is about 29.6% and 24.3%, respectively. Particles with a larger flow rate stay in the needle charger for a shorter time, resulting in less diffusion deposition of the particles on the charger wall. For the needle electrode wall, the deposition of particles with a diameter of 3 nm is less than 4% at different flow rates. Figure 8 shows the deposition axial distance (x_p/L) of the outer electrode wall as a function of the entrance radial position (r_p/r_1) for various particle diameters and flow rates. The deposition axial distance increases with the decrease in the entrance position in the needle charger. In other words, the particles collected by the outer electrode wall at the corresponding smaller entrance position indicate that the particles have larger particle diffusion depositions. Currently, the deposition distances for particles with a smaller entrance position are longer. The results show that the distance of the outer electrode wall affects the particle adhesion for different particle diameters and flow rates. In addition, for particles entering with the same position at various flow rates, the larger particles have a larger deposition distance because they are closer to the streamline and exhibit less diffusion deposition.

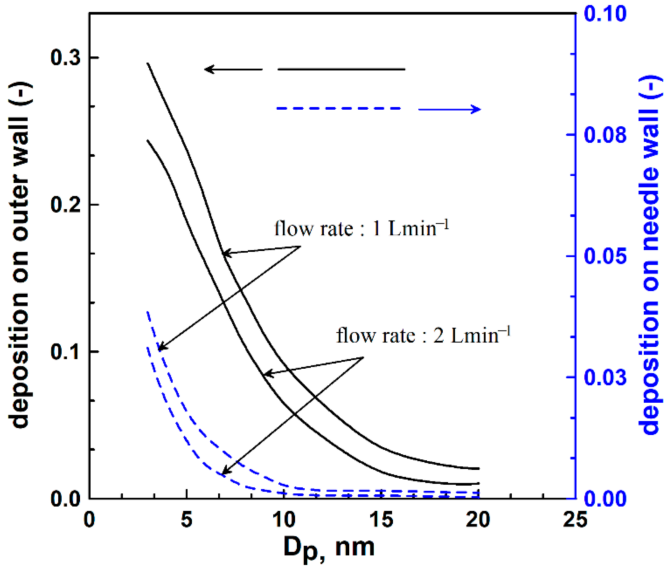

Figure 7. Comparison of particle deposition on the needle electrode wall and outer electrode wall.

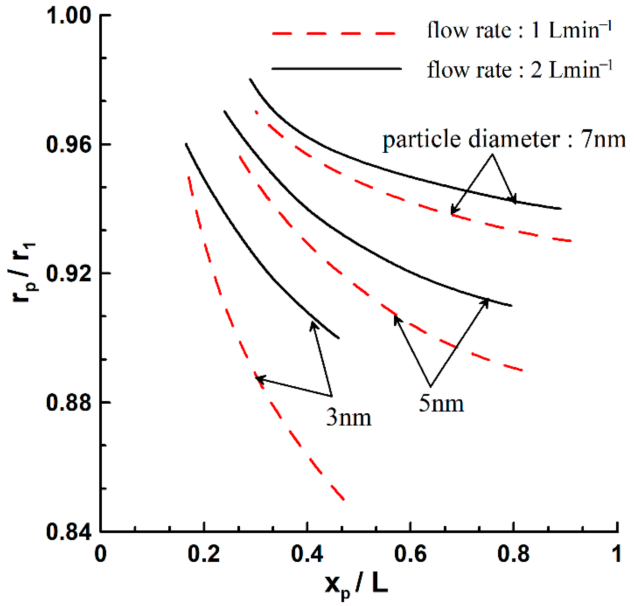

Figure 8. Entrance radial positions as a function of deposition axial distances for different particle diameters.

4. Conclusions

In this study, the ultrafine aerosol deposition in the needle charger was investigated by simulating the flow field and the particle trajectory. The proposed model allows quantitative calculation of the particle deposition as a function of flow rate and particle diameter for the needle charger without applied voltage. The calculations have been shown to agree with previously reported experimental data. This study also shows that an increasing flow rate reduces the particle deposition of the needle charger. It must be noted that the increase in flow rate also reduces the diffusion time of particles within the needle charger, which affects its intrinsic charging efficiency. From the attachment position of particle deposition, it demonstrates that most of the particles are attached to the outer electrode wall instead of the needle electrode wall for different flow rates and particle diameters. As the ultrafine aerosols are deposited on the outer electrode wall of the needle charger without applied voltage, the axial wall distance affects the particle deposition. For future research directions, it is recommended to carry out the numerical simulation of the intrinsic charging efficiency

and extrinsic charging efficiency of the needle charger. In addition, the model will be applied to investigate how to reduce nanoparticle adhesion, improve charging efficiency, and obtain the charge distribution of the charger under different conditions.

Author Contributions: Conceptualization, C.-H.H.; methodology, C.-H.H.; software, C.-H.H. and Y.-H.C.; validation, C.-H.H. and Y.-H.C.; formal analysis, C.-H.H. and Y.-H.C.; investigation, C.-H.H. and Y.-H.C.; resources, C.-H.H. and Y.-H.C.; data curation, C.-H.H. and Y.-H.C.; writing—original draft preparation, C.-H.H.; writing—review and editing, C.-H.H.; visualization, C.-H.H.; supervision, C.-H.H.; project administration, C.-H.H.; funding acquisition, C.-H.H. All authors have read and agreed to the published version of the manuscript.

Funding: This research was partially supported through the Ministry of Science and Technology of Taiwan under the contract number MOST 110-2622-8-009-012-TE5.

Institutional Review Board Statement: Not applicable.

Informed Consent Statement: Not applicable.

Data Availability Statement: Not applicable.

Conflicts of Interest: The authors declare no conflict of interest.

References

1. Morawska, L.; Ristovski, Z.; Jayaratne, E.R.; Keogh, D.U.; Ling, X. Ambient nano and ultrafine particles from motor vehicle emissions: Characteristics, ambient processing and implications on human exposure. *Atmos. Environ.* **2008**, *42*, 8113–8138. [CrossRef]
2. Bui, V.K.H.; Moon, J.Y.; Chae, M.; Park, D.; Lee, Y.C. Prediction of aerosol deposition in the human respiratory tract via computational models: A review with recent updates. *Atmosphere* **2020**, *11*, 137. [CrossRef]
3. Schraufnagel, D.E. The health effects of ultrafine particles. *Exp. Mol. Med.* **2020**, *52*, 311. [CrossRef] [PubMed]
4. Beauchemin, S.; Levesque, C.; Wiseman, C.L.S.; Rasmussen, P.E. Quantification and characterization of metals in ultrafine road dust particles. *Atmosphere* **2021**, *12*, 1564. [CrossRef]
5. Fierz, M.; Houle, C.; Steigmeier, P.; Burtscher, H. Design, calibration, and field performance of a miniature diffusion size classifier. *Aerosol Sci. Technol.* **2011**, *45*, 1–10. [CrossRef]
6. Shin, W.G.; Pui, D.Y.H.; Fissan, H.; Neumann, S.; Trampe, A. Calibration and numerical simulation of nanoparticle surface area monitor (TSI Model 3550 NSAM). *J. Nanopart. Res.* **2006**, *9*, 61–69. [CrossRef]
7. Qi, C.; Chen, D.R.; Pui, D.Y.H. Experimental study of a new corona-based unipolar aerosol charger. *J. Aerosol Sci.* **2007**, *38*, 775–792. [CrossRef]
8. Fierz, M.; Meier, D.; Steigmeier, P.; Burtscher, H. Aerosol measurement by induced currents aerosol measurement by induced currents. *Aerosol Sci. Technol.* **2014**, *48*, 350–357. [CrossRef]
9. Schriefl, M.A.; Nishida, R.T.; Knoll, M.; Boies, A.M.; Bergmann, A. Characterization of particle number counters based on pulsed-mode diffusion charging. *Aerosol Sci. Technol.* **2020**, *54*, 772–789. [CrossRef]
10. Romay, F.J.; Liu, B.Y.H.; Pui, D.Y.H. A sonic jet corona ionizer for electrostatic discharge and aerosol neutralization. *Aerosol Sci. Technol.* **1994**, *20*, 31–41. [CrossRef]
11. Aliat, A.; Tsai, C.J.; Hung, C.T.; Wu, J.S. Effect of free electrons on nanoparticle charging in a wire-tube negative corona discharge. *Appl. Phys. Lett.* **2008**, *93*, 154103. [CrossRef]
12. Tabrizi, N.S.; Ullmann, M.; Vons, V.A.; Lafont, U.; Schmidt-Ott, A. Generation of nanoparticles by spark discharge. *J. Nanopart. Res.* **2009**, *11*, 315. [CrossRef]
13. Marquard, A.; Meyer, J.; Kasper, G. Characterization of unipolar electrical aerosol chargers—Part II: Application of comparison criteria to various types of nanoaerosol charging devices. *J. Aerosol Sci.* **2006**, *37*, 1069–1080. [CrossRef]
14. Alguacil, F.J.; Alonso, M. Multiple charging of ultrafine particles in a corona charger. *J. Aerosol Sci.* **2006**, *37*, 875–884. [CrossRef]
15. Intra, P.; Tippayawong, N. Progress in unipolar corona discharger designs for airborne particle charging: A literature review. *J. Electrost.* **2009**, *67*, 605–615. [CrossRef]
16. Alonso, M.; Martin, M.I.; Alguacil, F.J. The measurement of charging efficiencies and losses of aerosol nanoparticles in a corona charger. *J. Electrost.* **2006**, *64*, 203–214. [CrossRef]
17. Tsai, C.J.; Lin, G.Y.; Chen, H.L.; Huang, C.H.; Alonso, M. Enhancement of extrinsic charging efficiency of a nanoparticle charger with multiple discharging wires. *Aerosol Sci. Technol.* **2010**, *44*, 807–816. [CrossRef]
18. Huang, C.H.; Alonso, M. Nanoparticle electrostatic loss within corona needle charger during particle-charging process. *J. Nanopart. Res.* **2011**, *13*, 175–184. [CrossRef]
19. Chien, C.L.; Tsai, C.J.; Chen, H.L.; Lin, G.Y.; Wu, J.S. Modeling and validation of nanoparticle charging efficiency of a single-wire corona unipolar charger. *Aerosol Sci. Technol.* **2011**, *45*, 1468–1479. [CrossRef]
20. Alonso, M.; Huang, C.H. High-efficiency electrical charger for nanoparticles. *J. Nanopart. Res.* **2015**, *17*, 332. [CrossRef]

21. Intra, P.; Wanusbodeepaisarn, P.; Siri-achawawath, T. Evaluation of the performance in charging efficiencies and losses of ultrafine particles ranging in sizes from 15 to 75 nm in a unipolar corona-based ionizer. *J. Electr. Eng. Technol.* **2021**, *16*, 963–974. [CrossRef]
22. Patankar, S.V. *Numerical Heat Transfer and Fluid Flow*; Hemisphere: Washington, DC, USA, 1980.
23. Hinds, W.C. *Aerosol Technology*, 2nd ed.; John Wiley & Sons, Inc.: Hoboken, NJ, USA, 1999.
24. Li, A.; Ahmadi, G. Dispersion and deposition of spherical particles from point sources in a turbulent channel flow. *Aerosol Sci. Technol.* **1992**, *16*, 209–226. [CrossRef]
25. Abouali, O.; Nikbakht, A.; Ahmadi, G.; Saadabadi, S. Three-dimensional simulation of brownian motion of nano-particles in aerodynamic lenses. *Aerosol Sci. Technol.* **2009**, *43*, 205–215. [CrossRef]